Int J Thermophys (2010) 31:1294–1309
DOI 10.1007/s10765-010-0746-4

An Apparatus Based on a Spherical Resonator for Measuring the Speed of Sound in Gases and for Determining the Boltzmann Constant

J. J. Segovia · D. Vega-Maza · M. C. Martín · E. Gómez · C. Tabacaru · D. del Campo

Received: 16 November 2009 / Accepted: 26 April 2010 / Published online: 13 May 2010

Abstract The Spanish Metrology Institute and the Research Group TERMOCAL of the University of Valladolid are involved in a European project for which the main target is the determination of the Boltzmann constant k_B. We have set-up an acoustic gas thermometer, which consists of a stainless steel spherical resonator, 4 cm nominal radio, in an adiabatic enclosure. The temperature stability and uniformity obtained are about 0.1 mK. This system allows performance of measurements of acoustic and microwave resonance frequencies. Microwave measurements characterize the resonator volume. Both hemispheres, joined by a flange in the equatorial band, can be misaligned up to 50 μm, splitting degenerate microwave modes in suitable triplets. Acoustic radial resonances in helium and argon can be used to compute the zero-density limit at the speed of sound at T_{TPW}. Kinetic theory of gases and hydrodynamics reveals k_B from this speed of sound value. In this article, a description of the apparatus and the first results using argon will be presented.

Keywords Boltzmann constant · Gas acoustic thermometry · Speed of sound

1 Introduction

The Spanish Metrology Institute (Centro Español de Metrología—CEM) in consortium with the Research Group TERMOCAL of the University of Valladolid (UVa) are

J. J. Segovia (✉) · D. Vega-Maza · M. C. Martín
Research Group TERMOCAL, Universidad de Valladolid, Paseo del Cauce 59, 47011 Valladolid, Spain
e-mail: josseg@eis.uva.es

E. Gómez · C. Tabacaru · D. del Campo
Centro Español de Metrología, Alfar 2, 28760 Tres Cantos, Madrid, Spain

involved in a European project for which the main target is the determination of the Boltzmann constant k_B.

The main objective of the project is the determination of the Boltzmann constant for the redefinition of the kelvin. The unit of temperature T is defined by the temperature of the triple point of water so it is linked to a material property. The purpose is to relate the unit to a fundamental constant and fix its value. For the kelvin, the corresponding constant is the Boltzmann constant k_B, because the temperature always appears as thermal energy $k_B T$ in fundamental laws of physics. Previously to fix its value, it must first be determined with an appropriate uncertainty to confirm the present value. The project coordinates promising experimental methods having the potential to contribute to new determinations of k_B.

The value of the molar gas constant R recommended by CODATA in 2006 is the weighted mean of only two independent results for the speed of sound in argon obtained at a temperature close to and known in terms of the triple point of water. One result is from the National Institute of Standards and Technology (NIST), USA, with a relative uncertainty $u_r = 1.7 \times 10^{-6}$, and the other from the National Physical Laboratory (NPL), UK, with $u_r = 8.4 \times 10^{-6}$. Although both values are consistent, because of the large difference in their uncertainties, the recommended value of R and k_B with $u_r(k_B) = 1.8 \times 10^{-6}$ [1], is determined only by the NIST result. This lack of independent data signifies that it is not possible to fix the value of k_B.

In order to improve the value of the Boltzmann constant for re-defining the kelvin, three different methods are used: acoustic gas thermometry, Doppler-broadening thermometry, and dielectric-constant gas thermometry. The partners of the project will determine the Boltzmann constant independently using different experiments.

The redefinition will endorse and encourage the use of both thermodynamic and International Temperature Scale of 1990 (ITS-90) temperatures and will also impact on uncertainties in thermodynamic temperature measurements. The Spanish team is contributing using acoustic gas thermometry. k_B will be re-determined by using the simple, exact connection between the speed of sound in noble gases (extrapolated to zero pressure) and the thermodynamic temperature T, the molar mass of the gas M, and the universal gas constant R. The speed of sound will be determined in a spherical cavity of known volume V by measuring the microwave resonance frequencies.

2 Principles of the Method

2.1 Acoustic Resonances

The principles of the acoustic thermometry and the spherical resonators have been described in the literature [1–8], so only a brief summary of the fundamentals is included in this section.

The speed of sound u in a real gas is given as a function of the density ρ:

$$u^2 = \left(\frac{\partial p}{\partial \rho}\right)_S = A_0 \left(1 + \beta_a \rho_n + \gamma_a \rho_n^2 + \cdots\right) \tag{1}$$

where the coefficients β_a, γ_a are the acoustic virial coefficients and A_0 is the value of the speed of sound when the density is zero and it is given by the equation:

$$A_0 = \frac{RT\gamma^{pg}}{M} \tag{2}$$

R is the universal gas constant, T is the thermodynamic temperature, γ^{pg} is the ratio of the isobaric and isochoric heat capacities for a perfect gas, and M is the molar mass. So both equations establish the link between the speed of sound and the thermodynamic temperature.

In a spherical resonator, the acoustic resonance frequencies f_N^a of the gas are measured and they are related to the speed of sound [3,5] through the expression,

$$f_N^a = \frac{u}{2\pi a_0} \times \frac{a_0}{a}\nu_N^a + \Delta f_N^a \tag{3}$$

where a is the radius at pressure p, a_0 is the zero-pressure radius, ν_N^a is an eigenvalue known exactly, and Δf_N^a is a sum of small correction terms; the subscript N indicates the mode of oscillation.

The most important contribution to the correction term is due to the thermal boundary layer near the wall resonator:

$$\Delta f_h = -(\gamma - 1)\frac{f}{2a}\delta_h\left(1 - \frac{2l_h}{\delta_h}\right) \tag{4}$$

The thermal penetration length δ_h is expressed as a function of the thermal diffusivity D_h, and the thermal accommodation length l_h depends on the thermal conductivity of the gas κ according to the following equations:

$$\delta_h = \left(\frac{D_h}{\pi f}\right)^{0.5} \qquad D_h = \frac{\kappa}{\rho c_p} \tag{5}$$

$$l_h = \frac{\kappa}{p}\left(\frac{\pi MT}{2R}\right)^{0.5}\left(\frac{2-h}{h}\right) \tag{6}$$

where h is the thermal accommodation coefficient at the wall of the resonator [9].

Other small contributions to the correction term of Eq. 3 take into account the coupling of gas and shell motion, Δf_{sm} [10] and the presence of the ducts, Δf_d [4]. The shell motion correction is evaluated from the elastic constants of the wall material [11,12].

2.2 Microwave Resonances

The measurement of microwave resonances is an accurate way to determine the thermal expansion of a cavity [2,13]. The volume of a cavity can indeed be determined if the nearly degenerate frequencies of a microwave multiplet are resolved sufficiently well that their average frequency can be measured accurately [14].

We restricted our analysis to the three first triply degenerate modes TM $1n$ and the three triply degenerate modes TE $1n$. The frequency range is 2.74 GHz to 10.9 GHz.

The average real u and imaginary v parts of the signal transmitted through the resonator were fitted to a sum of complex functions of the frequency [8]:

$$u + \mathrm{i}v = \sum_{m=0,\pm1} \frac{2\mathrm{i} f g_{1n}^{m} A_{1n}^{m}}{F_{1n}^{m^2} - f^2} + B + C\left(F_{1n}^{m} - f\right) \tag{7}$$

where A, B, and C are complex constants and $F_N = f_N + \mathrm{i}g_N$ are the complex degenerate resonance frequencies of the mode under study.

3 Experimental Setup

A schematic view of the gas acoustic thermometer is shown in Fig. 1. The apparatus has been designed based on the equipment of Trusler from Imperial College [15–17]. The setup consists of a stainless steel spherical resonator, 4 cm nominal radius, in an adiabatic enclosure.

The temperature stability and uniformity obtained are around 0.2 mK and 0.5 mK, respectively. This system can be used to perform measurements of acoustic and microwave resonance frequencies. Microwave measurements characterize the resonator volume. Acoustic radial resonances in helium and argon are used to compute the zero-density limit speed of sound at T_{TPW}. Kinetic theory of gases and hydrodynamics reveals k_{B} from this speed-of-sound value.

3.1 Resonator

The spherical resonator was built using two stainless-steel hemispheres fabricated from Type 316L stainless-steel bar stock. This material was selected because of its good machining properties. Both hemispheres, joined by a flange in the equatorial band, can be misaligned up to 50 μm, splitting degenerate microwave modes in suitable triplets. They form a cavity of 40 mm of nominal internal radius with a thickness of 10 mm. On the top of the spherical resonator is the inlet gas tube with a diameter of 1 mm and 40 mm long; there is another tube on the bottom which allows working with a small flow of gas to avoid accumulation of impurities inside the resonator.

Two transducer ports are drilled on the north part; and symmetrically on the south, there are another two ports. The microwave transducers are located on the north whereas the electroacoustic transducers are on the south part. All the o-rings are made of a perfluoroelastomer.

3.2 Transducers

Two acoustical transducers [17] and two antennas, non-commercial, are arranged on the cavity, sharing the same housing design. Electroacoustic transducers are known under the generic name of solid-dielectric capacitance transducers. The source and

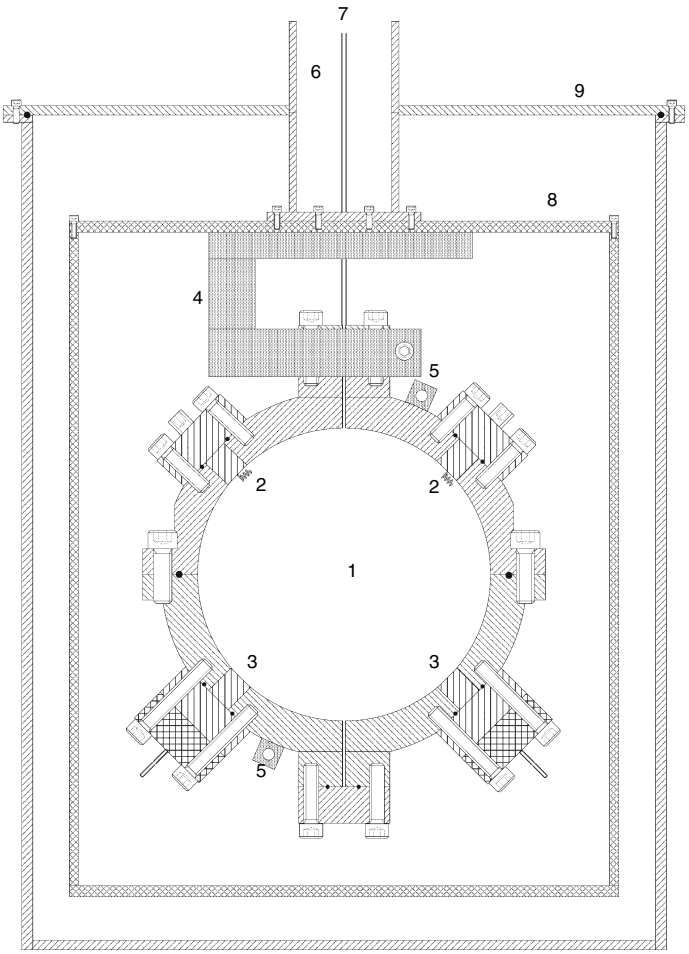

Fig. 1 Spherical resonator: 1—spherical resonator, 2—antenna, 3—electroacoustic transducer, 4—copper block, 5—thermometer (CSPRT), 6—to vacuum, 7—inlet tube, 8—isothermal shield, 9—vacuum jacket

detector present the same mechanical design, which are shown in detail in Fig. 2. The circular diaphragm is a 3 mm diameter active area, 12 μm thick polyimide film coated on one side with a layer of gold 49 nm thick. The diaphragms are placed nearly flush with the inner shell surface.

A synthesized excitation signal of frequency f (Hewlett-Packard HP3225 B), accurate to $\pm 1 \times 10^{-7}$, is fed to the source after amplification to 180 V rms but without the addition of a dc bias so that sound is produced at a frequency $2f$. A pre-amplifier, voltage gain set to unity, is located behind the detector, not close to the cavity to avoid power dissipation that perturbs the gradient temperature shape, connected to the detector with a tri-axial cable with an active guard. The purpose of the preamplifier is to buffer the signal from the detector transducer so that it may be measured by the lock-in amplifier (Stanford Research Systems SR850—100 kHz DSP) without placing

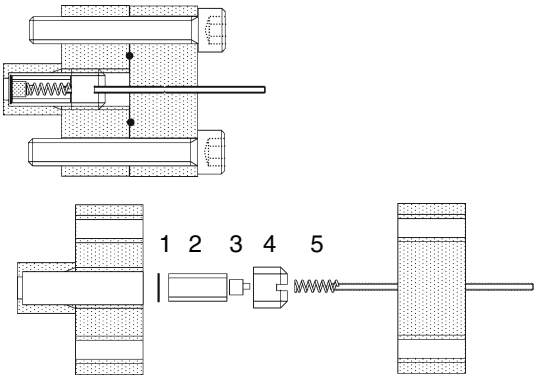

Fig. 2 Solid-dielectric capacitance transducer: 1—diaphragm, 2—glass sleeve, 3—back electrode, 4—screw, 5—spring contact

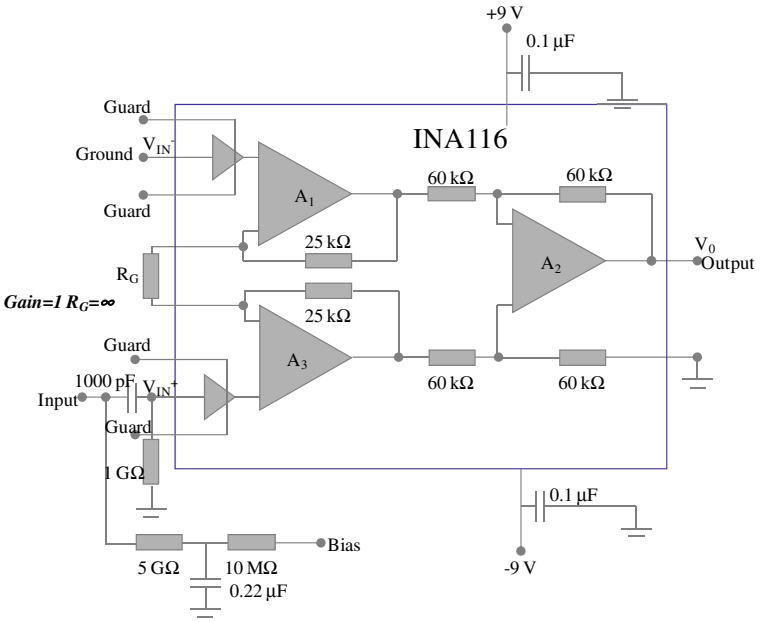

Fig. 3 High input impedance preamplifier scheme

a significant load on the transducer. The scheme is shown in Fig. 3. Typical detector signals are around 1 mV.

The antennas are built using an OFHC copper loop (0.125 mm diameter) for which electrical and magnetic fields are excited. Microwave resonance modes are swept with a Agilent network analyzer N5230C PNA-L, with a frequency range up to 13.5 GHz.

3.3 Thermostat

The thermostat has been designed for operation in a temperature range $T = (123$ to $523)$ K. The gas-inlet tube and the wires that enter down the central access tube are

thermally anchored to the large copper block from which the resonator is suspended. The temperature of the copper block is controlled by means of a heater and a platinum resistance thermometer (CSPRT Rosemount 162D), and it is maintained at the set temperature of the resonator.

The thermostat of the resonator is controlled in different stages. Primary temperature control is done on the smaller copper block, in which the upper boss of the sphere is clamped, using a thermometer and heater mounted in it. The thermometer is read every 5 s using a multimeter (Hewlett-Packard HP3458A) and a switch control unit (Agilent Technologies 3499B). The copper post interconnecting the two blocks provided a controlled heat leak.

The side and base of the isothermal shield surrounding the sphere are separately controlled at the set temperature. The thermostat operates under vacuum to reduce heat transfer between the resonator and the shield. Moreover, heat losses from the shield are reduced using layers of aluminum foil separated by glass-fiber tissue. The temperature control loops are programmed in the computer using again the multimeter HP3458A and the switch control unit A3499B, and programmable power supplies (Hewlett-Packard E3632A). When the equipment works below ambient temperature, the apparatus is immersed in a Dewar vessel filled with ethanol which is maintained at a constant temperature through an external recirculating thermostat (Julabo F81ME) which is 10 K below the set point of the sphere.

The mean temperature of the gas is obtained from readings of two capsule-type platinum resistance thermometers (CSPRT Rosemount 162D) using an ac bridge ASL F18. The thermometers are mounted in copper blocks attached to the outer surface of the resonator, one on the north and the other on the south. They are calibrated on ITS-90 and traceable to national standards. Temperature stability is excellent, and drifts for measurements are much less than 1 mK. The estimated overall uncertainty is 0.19 mK for a coverage factor $k = 1$; the details are given in Table 1.

A temperature gradient of 0.1 mK was present across the resonator during the acoustic measurements. Imperfections on the measurement of the temperature itself are estimated to be 0.19 mK. Both contributions gives an estimated uncertainty of approximately 0.8 ppm on k_B.

3.4 Pressure

The pressure of the gas is measured with an uncertainty of 100×10^{-6} Pa/Pa in the external tubing using a resonant quartz-crystal manometer (Digiquartz Model

Table 1 Temperature uncertainty budget

	Estimate (mK)	Distribution	Contribution to the standard uncertainty $u_i(T)$ (mK)
Stability	0.2	$\sqrt{12}$	0.06
Uniformity	0.5	$\sqrt{12}$	0.16
Calibration	0.07	1	0.07
Temperature		$k = 1$	0.19

2300A-101). It is calibrated in the pressure range from 0 MPa to 2 MPa traceable to national standards. The pressure measurements are corrected taking into account the level difference between the pressure transducer and the center of the sphere and the temperature gradient in the external tubing.

3.5 Gas Sample

The argon used for the acoustic measurements was from Air Liquid Alphagaz 2Ar (stated molar purity 99.9999 %). The supplier's lot analysis provided the following upper bounds for impurities: $H_2O \leq 0.5$ ppm, $O_2 \leq 0.1$ ppm, $CO_2 \leq 0.1$ ppm, CO $\leq$ 0.1 ppm, $C_mH_n \leq 0.1$ ppm, $H_2 \leq 0.1$ ppm. Prior to filling the resonator, the whole cavity assembly (shell, transducers…) was evacuated and vacuum baked at 150 °C during 48 h. Information provided by the supplier indicated that all specified impurities were less than 1×10^{-6} The maximum combined effect of the impurities on the argon sample is estimated to be less than $\pm 1 \times 10^{-6}$ on k_B.

4 Characterization of the Capsule Standard Platinum Resistance Thermometers

Capsule-type standard platinum resistance thermometers (CSPRTs) are used to measure the temperature in the north and south hemispheres of the resonator. To trace the temperature of the resonator to that of the triple point of water, the CSPRTs have to be calibrated in a triple-point-of-water cell realizing the best SI value for the present definition of the kelvin.

But one question arises from this calibration due to the fact that the conditions in which it is carried out are different from the way in which the CSPRTs are going to be used. That is to say, the behavior of the thermometers in a usual triple-point-of-water cell could be different from that expected in the resonator, mainly due to the surroundings: vacuum in the resonator while oil is normally used to immerse the thermometers which are calibrated in triple-point-of-water cells.

To characterize the sensors, and to study their behaviors in different environments, a special artifact to assemble the thermometers, allowing their measurement in the triple-point-of-water cells, was designed and constructed of stainless steel (see Fig. 4). The purpose of the artifact is to simulate the measurement conditions of the CSPRTs in the resonator. At the same time, it allows their calibration using the same wires used in the resonator and different gases at a controlled pressure, vacuum and oil in order to study the possible differences in the thermometer readings. The dimensions of the artifact are such that, except its head, it is fully immersed in the cells. In its bottom there is a copper bushing similar to one used in the resonator to hold the thermometers in their holes. To avoid heat conduction, the wires are coiled and thermally anchored inside the stainless steel sheath. Two different CSPRTs models, one of them metal-sheathed and the other one glass-sheathed, from two different manufacturers were characterized; Fig. 5 shows the change in the temperature recorded by the thermometers with respect to the change of the immersion depth of the assembly in the cell in vacuum (pressure at about $\sim 10^{-4}$ mbar), where 0 cm was chosen as a reference. Due to the better heat

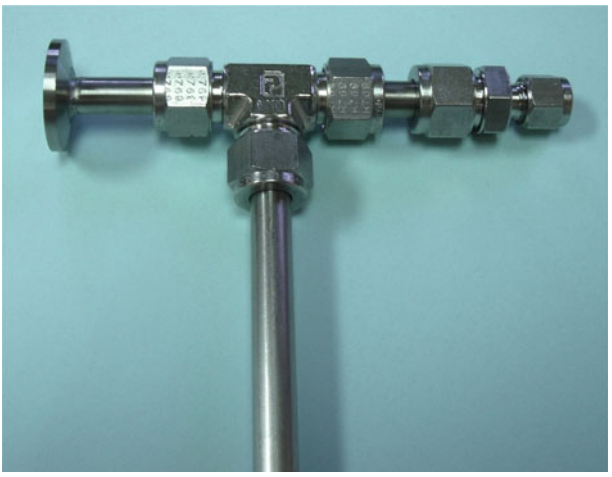

Fig. 4 Stainless-steel artifact used to characterize and calibrate the CSPRT, details of the top

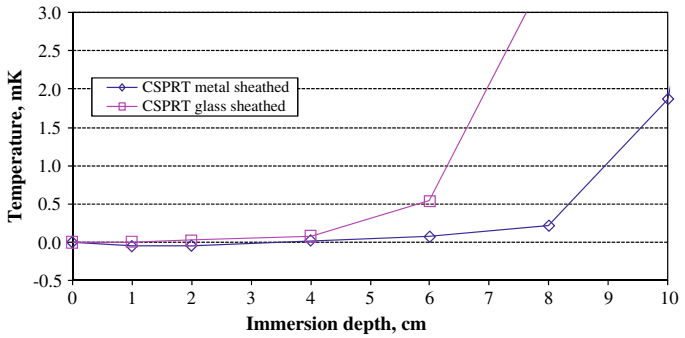

Fig. 5 Immersion depth in vacuum ($\sim 10^{-4}$ mbar) of the two models of CSPRTs mounted in the stainless-steel artifact immersed in a triple-point-of-water cell

conduction of the metal sheath in comparison with the glass sheath, the response of this thermometer to the change in the immersion depth is, in consequence, better. But for both cases, from Fig. 5, it can be concluded that along the first centimeters the heat conduction error in vacuum is negligible for both thermometers.

Also, measurements in oil, vacuum, argon, and helium at 300 mbar and 900 mbar were carried out. Each day, measurements in these four different media were performed at two different currents, 1 mA and $\sqrt{2}$ mA, in order to correct them for self-heating. The CSPRTs were maintained in their assemblies (see Fig. 4) during the measurements in vacuum or gas. To perform the measurements in oil, the CSPRTs were carefully dismounted and introduced in a similar stainless steel sheath as the one used in the previous assembly but filled with pre-cooled mineral oil. Figures 6 and 7 show the self heating values obtained on different measurement days. As expected, self-heating in the metal-sheathed thermometer is about three times smaller than in the glass-sheathed thermometer because metal favors heat dissipation. It can be seen too in Figs. 6 and 7 how the measurements in oil are more repetitive than in other media, especially in

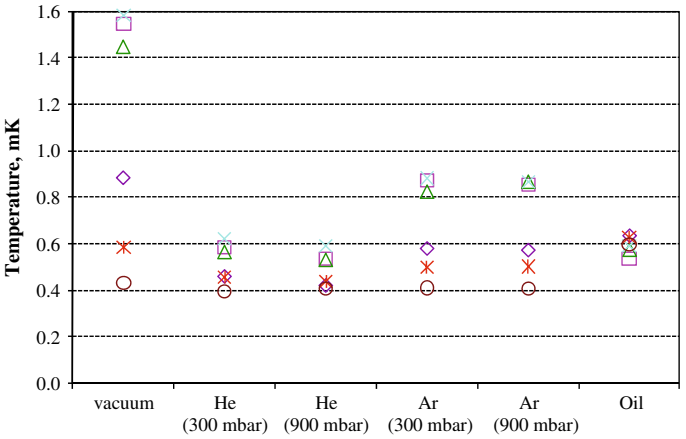

Fig. 6 Self-heating values obtained along different measurement days with the glass-sheathed thermometer

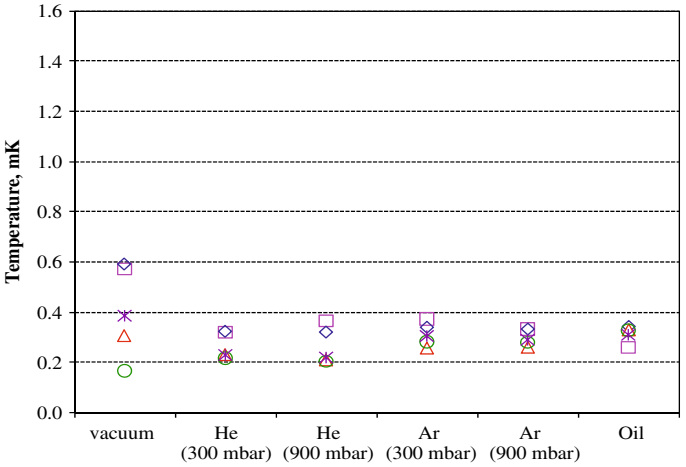

Fig. 7 Self-heating values obtained along different measurement days with the metal-sheathed thermometer

vacuum where the dispersion of the results are between 2 and 4 times larger than in oil. Figure 6 also shows how the glass-sheathed thermometer is more sensitive to the heat conduction of the media than the metal-sheathed one, because its self-heating in helium is smaller than in argon which has a smaller thermal conductivity. Therefore, if we based our decision in the self-heating measurements, it would be better to opt for the metal-sheathed thermometer which has the smallest and repetitive self-heating values. But if we plot the differences in the resistance values, corrected for self-heating (0 mA), measured at the triple point of water with respect to the results in oil for both thermometers, the decision will be just the opposite. Figures 8 and 9 show how the resistance values at 0 mA for the glass-sheathed CSPRT are more repetitive, less disperse, and coherent among the different fluids used to make the thermal contact.

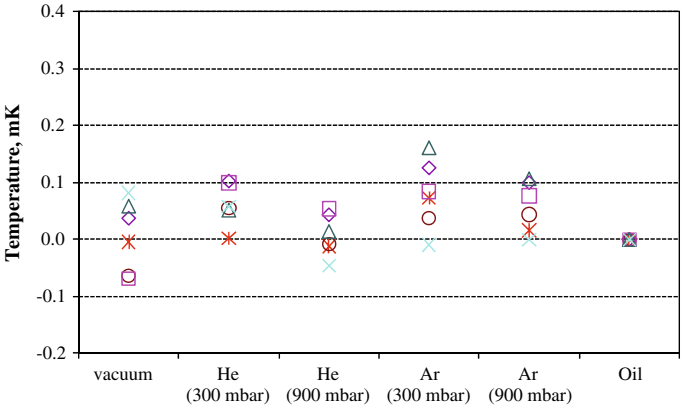

Fig. 8 Differences in the resistance values, corrected for self heating (0 mA), measured at the triple point of water with respect to the results in oil for the glass-sheathed CSPRT

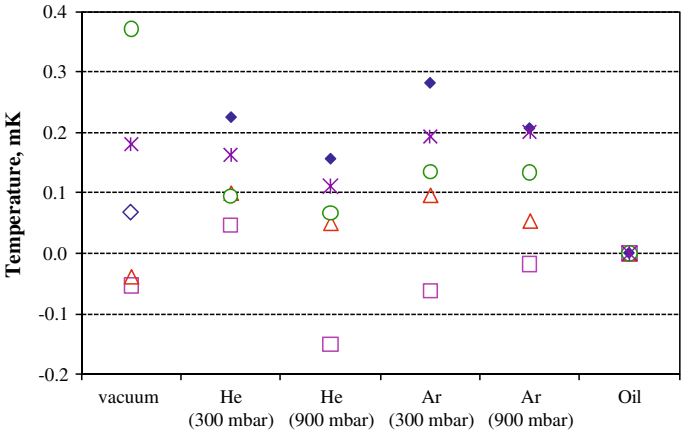

Fig. 9 Differences in the resistance values, corrected for self-heating (0 mA), measured at the triple point of water with respect to the results in oil for the metal-sheathed CSPRT

In conclusion, these characterization studies show that the more appropriate thermometer is the glass-sheathed one.

5 Acoustic Measurements

The frequencies and half-widths of the lowest six acoustic radial modes, designated as $(0, n)$, $n = 2, \ldots, 7$ have been measured. The gas is admitted into the resonator at pressures up to 1 MPa; one isotherm has been performed at 273.16 K. The pressure has been decreased in 0.1 MPa steps to the value of 0.1 MPa. The modes (0, 6) and (0, 7) have been discarded because the excess half-widths ($\Delta g/f$) are too high. The calculated excess half-widths on the (0, 6) mode are eight times higher than the excess half-widths of the (0, 2), (0, 3), (0, 4), and (0, 5) modes. The (0, 7) mode shows excess

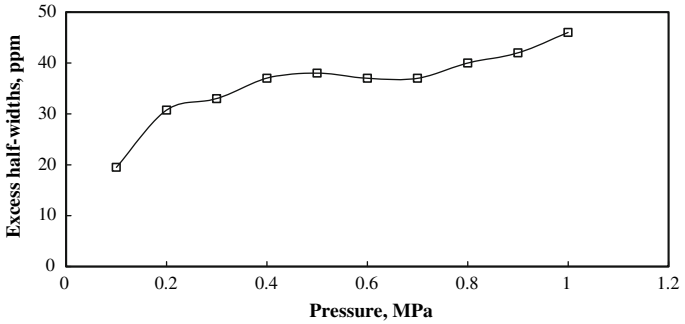

Fig. 10 Excess half-widths (relative to frequency differences between measured half-widths and calculated half-widths from theoretical model) versus pressure at 273.16 K, mode (0, 3)

half-widths four times higher than the excess half-widths of these first modes. The current cavity offers linear extrapolations of the excess half-widths to zero pressure equivalent to 20 ppm in k_B, a measure of our imperfect understanding of this acoustic resonator (Fig. 10). These unpredicted energy losses suggest that the surface finished of the current cavity is not suitable to decrease our uncertainties. A new well-polished cavity should provide a new uncertainty assessment (see Table 2).

The method used to measure the resonance frequencies f_N and half-widths g_N is the same used by other authors [4]. The source transducer is driven at 11 frequencies, from $f_N - g_N$ to $f_N + g_N$. Then it is reduced in steps back to its original value. At each frequency, the in-phase component u and the quadrature component v of the signal are measured and stored for analysis.

The measured resonance frequencies are corrected as has been explained in Sect. 2. They take into account the effect of the thermal boundary layer (the thermal accommodation coefficient $h = 0.93$) [1]. This correction is shown in Fig. 11 where the frequency shift due to the thermal boundary layer is represented as a function of the frequency at different pressures.

Other small contributions to the correction term of Eq. 3 take into account the coupling of gas and shell motion, Δf_{sm} which is represented in Fig. 12 as a function of the frequency at different pressures. We have determined the expected mode frequency theoretically, based on equations for a thick, spherical shell, and published values for the elastic properties of stainless steel [11,12]. The expected breathing mode frequency is 27978.5 Hz. The correction due to the presence of the ducts, Δf_d, is shown in Fig. 13.

The fitting precision of the resonance frequencies is less than 0.1 ppm for these resonance frequencies. Repeated measurements indicate that the precision of u/a_0 at a single point is approximately 0.6 ppm on this measurement.

There are systematic uncertainties arising from the values of the thermophysical properties used in calculation of the corrections to the measured resonance frequencies. We combine the standard errors obtained from the variance–covariance matrix with estimates of the systematic effect propagated from the uncertainties in the values used for the thermal conductivity k and the thermal accommodation coefficient h. These effects were estimated numerically by repeating the entire analysis using

Table 2 Resonance frequencies and half-widths for Ar near T_{TPW} for (0, 2), (0, 3), (0, 4), and (0,5) radial modes

$T = 273.1650$ K, $p = 1000.00$ kPa		$T = 273.1600$ K, $p = 900.07$ kPa		$T = 273.1620$ K, $p = 800.07$ kPa		$T = 273.1640$ K, $p = 700.05$ kPa	
f (Hz)	g (Hz)	f (Hz)	g (Hz)	f (Hz)	g (Hz)	f (Hz)	g (Hz)
5508.9855	0.8654	5507.9304	0.8546	5506.9934	0.8451	5506.1192	0.8501
9471.5174	1.0790	9469.7766	1.0825	9468.1906	1.0902	9466.7000	1.0914
13371.0788	1.0187	13368.6439	1.0599	13366.4280	1.0997	13364.3343	1.1580
17248.9006	1.7058	17245.7754	1.7301	17242.9364	1.7476	17240.2740	1.7918
$T = 273.1590$ K, $p = 600.04$ kPa		$T = 273.1630$ K, $p = 500.00$ kPa		$T = 273.1590$ K, $p = 400.01$ kPa		$T = 273.1560$ K, $p = 299.99$ kPa	
f (Hz)	g (Hz)	f (Hz)	g (Hz)	f (Hz)	g (Hz)	f (Hz)	g (Hz)
5505.1656	0.8723	5504.3538	0.9165	5503.4620	0.9812	5502.5649	1.0899
9465.0890	1.1671	9463.6769	1.2473	9462.1257	1.3576	9460.5532	1.4679
13362.0908	1.2450	13360.1175	1.3185	13358.0157	1.4568	13355.9363	1.6580
17237.4224	1.8570	17234.9096	1.9876	17232.2402	2.1463	17229.6234	2.4060
$T = 273.1600$K, $p = 199.95$kPa				$T = 273.1624$K, $p = 99.94$kPa			
f (Hz)		g (Hz)		f (Hz)		g (Hz)	
5501.6791		1.2880		5500.5288		1.7324	
9459.1306		1.6688		9457.4588		2.2211	
13353.9682		1.9947		13351.6987		2.7472	
17227.1758		2.8549		17224.4268		3.9271	

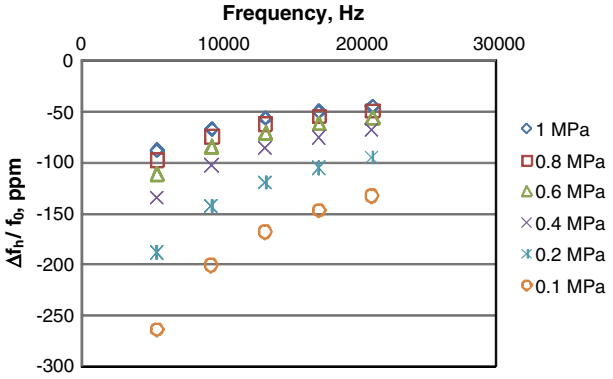

Fig. 11 Frequency shift due to the thermal boundary layer; Ar gas, stainless-steel 316L sphere: $T = 273.16$ K, radius = 40.011 mm, thickness = 10.0 mm

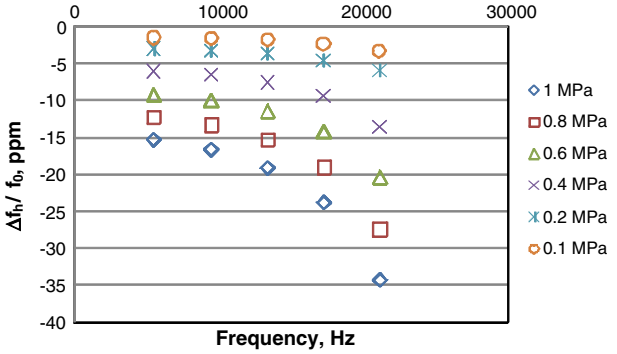

Fig. 12 Shell motion correction, shift in radial mode frequencies due to shell motion: Ar gas, stainless-steel 316L sphere, $T = 273.16$ K, radius $= 40.011$ mm, thickness $= 10.0$ mm

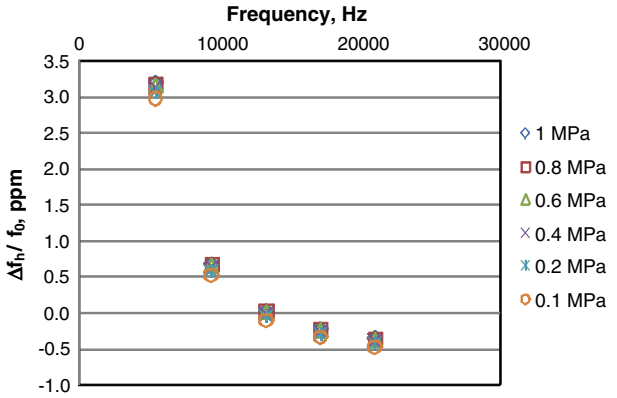

Fig. 13 Frequency perturbation: inlet and outlet duct, $r = 0.5$ mm, $L = 40$ mm

perturbed values of k and h. We considered it for the zero-pressure limit of the speed of sound, with an estimated value of 6 ppm on k_B.

6 Microwaves Measurements

The resonator volume is characterized by microwave measurements. Misaligned hemispheres lift the degeneracy of the modes, making it possible to fit the data to suitable triplets. The estimated uncertainty in the determination of the radius of the cavity with this technique is 10 ppm in k_B with the current cavity and configuration. We have recorded 201 frequencies of the six modes under study. They are the average of 10 scans with an IF bandwidth of 10 Hz. The network analyzer is configured to measure the scattering coefficient S_{21} for subsequent data analysis. This is calibrated with a standard calibration kit. Figure 14 shows measurements of the magnitude of the microwave signal detected as a function of frequency for mode TE 11 at 273.16 K. The deviations of experimental data from a fit (Eq. 7) are given in Fig. 15. The

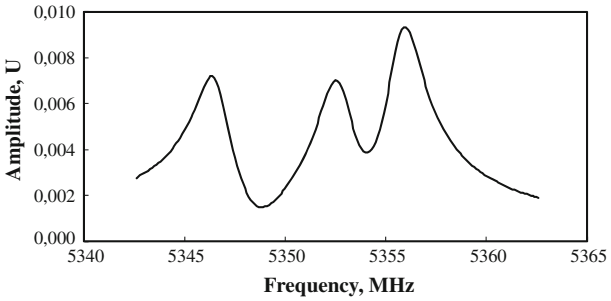

Fig. 14 Measurements of the in-phase and quadrature microwave signal detected as a function of frequency for mode TE 11 at 273.15 K

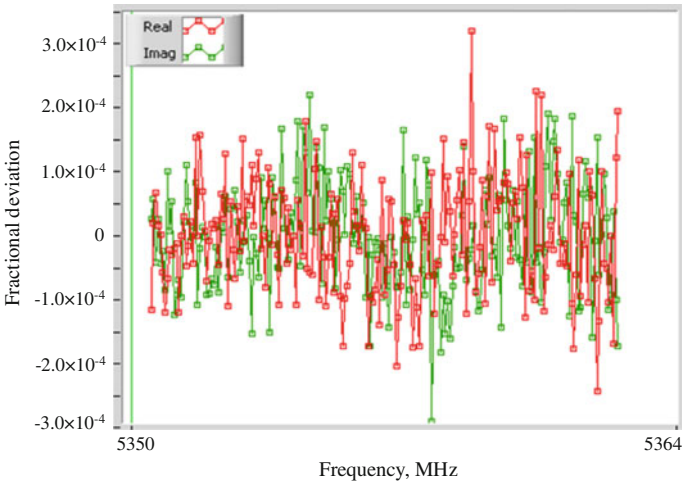

Fig. 15 Deviations of experimental data for a fit with three terms (triplet) in Eq. 7

fitting procedure is a Levenberg–Marquardt method. It's really a three-term fit, with 16 parameters (actually 15 because there are only two phase differences between the three components) [7]. The misaligned hemispheres split degenerate modes in suitable triplets.

7 Conclusions

This report presents the work progress at CEM-UVa, where we have started with a setup of a misaligned spherical resonator. The characterization of the CSPRT thermometers and the uncertainty in the temperature measurement have been performed; this is 0.19 mK ($k = 1$).

All the acoustic corrections have been evaluated at the experimental conditions, and the first results for the microwave measurements have been included.

The combined uncertainty expected for k_B is about 23 ppm.

Acknowledgment The work within this EURAMET joint research project leading to these results has received funding from the European Community's Seventh Framework Programme, ERA-NET Plus, under Grant Agreement No. 217257.

References

1. M.R. Moldover, J.P.M. Trusler, T.J. Edwards, J.B. Mehl, R.S. Davis, J. Res. Natl. Bur. Stand **93**, 85 (1988)
2. M.R. Moldover, S.J. Boyes, C.W. Meyer, A.R.H. Goodwin, J. Res. Nat. Inst. Stand. Technol. **104**, 11 (1999)
3. H. Plumb, G. Cataland, Metrologia **2**, 127 (1966)
4. M.R. Moldover, J.B. Mehl, M. Greenspan, J. Acoust. Soc. Am. **79**, 253 (1986)
5. M.R. Moldover, J.P.M. Trusler, Metrologia **25**, 165 (1988)
6. J.P.M. Trusler, *Physical Acoustics and Metrology of Fluids* (Adam-Hilger, Bristol, 1991), p. 253
7. M.B. Ewing, J.P.M. Trusler, J. Chem. Thermodyn. **32**, 1229 (2000)
8. G. Benedetto, R.M. Gavioso, R. Spagnolo, P. Marcarino, A. Merlone, Metrologia **41**, 74 (2004)
9. M.B. Ewing, M.L. McGlashan, J.P.M. Trusler, Metrologia **22**, 93 (1986)
10. J.B. Mehl, J. Acoust. Soc. Am. **78**, 782 (1985)
11. H.M. Ledbetter, Cryogenics **22**, 653 (1982)
12. S.L. Hoyt (ed.), *ASME Handbook on Metal Properties* (McGraw-Hill, New York, 1990)
13. M.B. Ewing, J.B. Mehl, M.R. Moldover, J.P.M. Trusler, Metrologia **25**, 211 (1988)
14. J.B. Mehl, M.R. Moldover, Phys. Rev. A **34**, 3341 (1986)
15. J.F. Estela-Uribe, J.P.M. Trusler, C.R. Chamorro, J.J. Segovia, M.C. Martín, M.A. Villamañán, J. Chem. Thermodyn. **38**, 929 (2006)
16. J.P.M. Trusler, M. Zahari, J. Chem. Thermodyn. **24**, 973 (1992)
17. A.F. Estrada-Alexanders, J.P.M. Trusler, J. Chem. Thermodyn. **27**, 1075 (1995)